

Nanocrystalline Porous Thin Film VN_x Hydrogen Absorbents: Method of Production, Structure and Properties

Alexey Guglya^{1*}, Alexander Kalchenko¹, Elena Solopikhina¹, Viktor Vlasov¹ and Elena Lyubchenko²

¹ National Science Center “Kharkov Institute of Physics and Technology”, Kharkov, Ukraine

² National Technical University «Kharkov Polytechnic Institute”, Kharkov, Ukraine
Email: guglya@kipt.kharkov.ua

Abstract. Vanadium and its alloy-based hydrides are extensively studied with regard to their use as hydrogen absorbents. The ion beam-assisted deposition method (IBAD) used for nanocrystalline VN_x - H_y thin-film hydrogen storages production is analyzed. The data of transmission and scanning electron microscopic studies of all stages of the film formation are considered. The main mechanisms of intergranular pores formation in nanograin structures have been established. The relation between the parameters of the ion beam-assisted deposition and those of film structure has been shown. The obtained data provide the explanation of the mechanisms of hydrogen absorption and desorption by thin films. It was suggested that the availability of branched network of intergranular pores allows accumulating the hydrogen by VN_x - H_y nano structures in large quantities and release it at the temperatures less than 275°C.

Keywords: Nanocrystalline structures; hydrogen; storage; thin films; ion-beam assisted deposition.

1 Introduction

Vacuum deposition techniques, such as magnetron sputtering, physical and chemical vapor deposition, have been successfully used for thin films deposition for a long time. A characteristic feature of these techniques is that the resulting structures are formed under less than equilibrium conditions allowing the creation of materials with unique properties.

B.Movchan and A.Dymchishin in 1969 [1] have shown the substrate temperature influence on the structure of Ti, Ni, W, ZrO_2 , and Al_2O_3 films. Evaporation of the substances was carried out by the electron beam heating of the crucible. Three temperature zones with boundary temperatures T_1 and T_2 , that are respectively equal to 0.3 and 0.45 ... 0.5 of T_m for metals, 0.22 ... 0.26 and 0.45 ... 0.5 of T_m for oxides were determined. The films with certain structure and properties have been formed inside each of these zones. These studies marked the beginning of the so-called structure zone model (SZM). Later J. Thornton [2] took into account the effect of the gas environment on the film structure additionally to the influence of the substrate temperature. It was shown that the film formation mechanism during ion bombardment was fundamentally changed not only by substrate temperature but also by pressure of the working gas (argon). Effect of the reactive gas (oxygen) on the formation of the microstructure of thermally evaporated metal (in that case, aluminum) has been studied in detail by P. Barna and M. Adamik [3]. Oxygen adsorbed on the surface during deposition reduces the mobility of grain nucleating centers and inhibits their coalescence. It results in the breaking of the columnar structure and nucleation of the grains with different texture. Eventually, at a high concentration of oxygen molecules, formation of aluminum oxide matrix with metallic inclusions is observed.

The substrate temperature and gas concentration influence the formation of the film structure only at the initial stage. At this stage, the density of nucleation centers is determined mainly by the surface diffusion coefficient. For equiaxial nanocrystalline structure formation, it is necessary to speed up the bulk diffusion in the film at its growth stage. It can be achieved by ion-stimulation processing of the film.

During the bombardment of the deposited film by 0.02-2 keV energy ions, generation of radiation-induced defects not more than 1-10 displacements per atom takes place. It gives the intensification of diffusion processes and the introduction of gas ions to a depth of 5-10 nm. As a result, we observed

reduced intergranular porosity and increased density of the film. The additional spaces for the grains nucleation appear on the surface of the growing film, which in turn leads to grain size decrease and inhibition of columnar structure growth [4, 5].

However, the best opportunities for the nanocrystalline films formation arise if the substrate is bombarded by gas ions of energies more than 10 keV during the metal vapor deposition. This combination of metal evaporation with the ion irradiation is implemented in the ion beam-assisted deposition technology (IBAD) method [6-10]. Ions with such energies create a large number of defects, on which the grain nuclei are formed. Consequently, the nanocrystalline structures with grain size that does not exceed 10 nm are formed [9-11].

Hydrides on the base of vanadium, a light transition metal, are considered to be perspective for usage as solid state hydrogen storages. The total mass of stored hydrogen in them reaches the value of 2.1 wt.%. The amount of absorbed hydrogen atoms in VH_2 is essentially more than other hydrides, for example, in MgH_2 hydride (11.2 in VH_2 vs. 2.5 wt.% in MgH_2 , at./ cm^3 , $\times 10^{22}$) [12].

V-H system includes the following phases: α - solid solution; β - ($\text{VH}_{0.45}$ - $\text{VH}_{0.95}$) and γ - VH_2 . The $\beta + \gamma$ phase mixture is in the $\text{VH}_{1.0}$ - $\text{VH}_{2.0}$ concentration range. The V_2H , V_3H_2 and V_4H_3 ordered structures are revealed in the homogeneity range of the β -phase. The β -phase has the body-centered tetragonal lattice (bct), the $\text{VH}_{1.77}$ non-stoichiometric phase has fcc lattice.

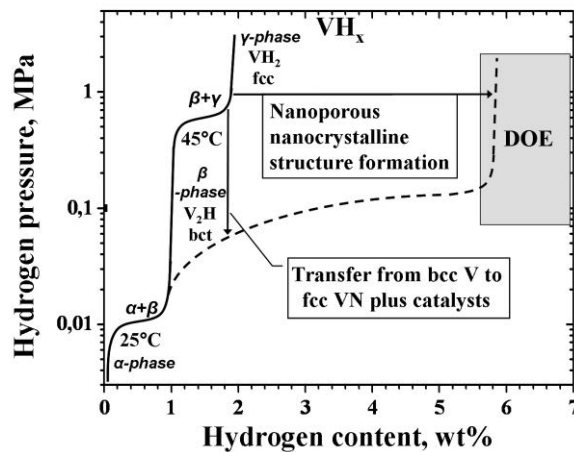


Figure 1. Pressure-concentration constitution diagram for hydride VH_x (summarized data from [13]). Dot line is related to the state when this hydride may be used as hydrogen storage.

Due to the existence of several V-H phases with different crystal structures several plateaus related to the phase transitions have to appear on the P-C-T diagram (Fig. 1). The figure also shows the possible ways of the improvement of the absorptive properties of vanadium hydride, such as nano-porous structure formation (increasing of the gravimetric capacity); hydride phase stabilization by means of complex VN_xH_y hydride formation and development of the additional hydrogen traps (the improvement of the thermodynamic and kinetic properties).

The aim of this study is to investigate the structure and desorption characteristics of V-N films prepared using the ion beam-assisted deposition technology.

2 Experimental procedure

Nanocrystalline VN_x porous thin films were obtained by evaporation of vanadium from electron-beam crucible at the simultaneous irradiation by a mixed beam of helium and nitrogen ions ($\text{N}_2^+/\text{He}^+=1$) with energy of 30 keV. The ratio between the speeds of vanadium atoms deposition and gas ion implantation was 0.5at./ion. The film deposition was conducted onto the NaCl substrate at 200°C. Thin carbon film was deposited on the substrate before the vanadium evaporation. During the vanadium film deposition

the parts of the substrate were sequentially overlapped by shutter at regular time intervals. The set of films with a thickness from 5 up to 25 nm was obtained.

In addition, films of 1.5 μm thickness and $1.5 \times 1.5 \text{ cm}$ area were deposited on sapphire and silicon substrates. The structure of the films deposited on silicon and NaCl substrates was investigated by means of JEM 100CX transmission and JSM 7001F scanning electron microscopes.

3 The results of the experiments

3.1 The initial stage of film formation

The inhomogeneity zone is always observed in the surface layer of deposited film at its bombardment by gas ions with energy of some tens of keV. The number of generated defects and implanted gas concentration are increased successively deep inside the zone starting from the film surface. The extent of this zone is determined by the path depth of ions used for the bombardment of deposited material. For example, an extent of this heterogeneity zones for 30 keV-nitrogen ions is $\sim 70\text{-}80 \text{ nm}$ [6]. Accordingly, the structure of the film at the nucleation stage and after its thickness has exceeded 80 nm, is different. Therefore, the zone of structural heterogeneity seems to be a good subject for investigation of the mechanisms of nano-porous structure formation at the bombardment by medium-energy gas ions.

Using SPURT program as described previously [14], we performed a mathematical modeling of the defect formation (Fig. 2a) and ion implantation of nitrogen and helium (Fig. 2b) processes in the deposited vanadium film.

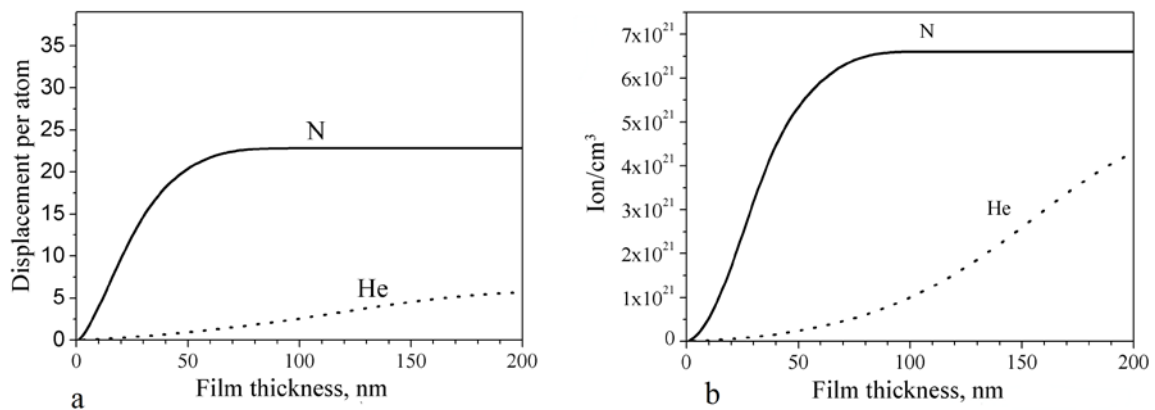


Figure 2. Thickness dependencies of damage distribution (displacement per atom) (a) and implanted helium and nitrogen atoms (b) in the V-N-He film. $j(\text{N}_2^+, \text{He}^+) = 10^{14} \text{ ion/cm}^2 \cdot \text{sec}$.

Fig. 2, a shows that the most of the damages in the film at all stages of deposition arise from the nitrogen ions. Moreover, the impact of nitrogen ions on the structure and composition of the vanadium film ends at a depth of 80 nm. The level of damages at thicknesses more than 80 nm increases slightly due to helium ions exclusively. The quantity of implanted nitrogen at such thicknesses is not changed; and helium concentration increases almost tenfold. At a depth of 250 nm the calculated concentration of helium in vanadium film is similar to nitrogen concentration at a depth of $>80 \text{ nm}$, namely, $6.5 \cdot 10^{21}$ ions/cm³ (it has not been shown in the Fig.2). Thus, calculations show that the structure and composition of the film of less than 80 nm-thicknesses are determined by the concentration and amount of radiation defects generated by nitrogen ions. In the thickness range of 80-250 nm the film structure can be transformed due to implanting helium ions. Total estimated amount of nitrogen and helium in the vanadium film of thickness $> 250 \text{ nm}$ should not exceed 12.0 at.%.

Fig. 3 shows the electron-microscopic images of VN_x films at the initial stage of their growth. Fig. 3, e demonstrates the same piece of the 20 nm-thickness film as the Fig. 3, d but at different electron beam focusing. Fig. 3, e shows the image of new grains inside the ruptures. All figures present the negative

images for better visualization of the grain boundaries and pores. It is seen that the films are solid even at a thickness of 5 nm. They have a nanocrystalline structure with grain size of 10-15 nm. Grains are arranged in a single layer; 3-5 nm pores are observed almost in all triple and quadratic intergranular joints.

Specific ruptures of 100 nm length and ~10-15 nm width appear in film starting from the thicknesses of 15 nm (Fig. 3, c) and there are large (~ 50-150 nm) areas (hereinafter referred to as blocks) that are visible between the adjacent ruptures. Blocks display heterogeneous structures and consist of nano grains separated by porous boundaries. Filling the ruptures by the grains of new population (Fig. 3, e, f) takes place simultaneously with the subsequent layers formation. Their average size is approximately the same as the size of the grains inside the particle, namely, ~ 15-20 nm. At film thicknesses more than 30-40 nm the ruptures are completely filled by nano grains and formation of subsequent layer of particles and grains begins.

The crystal structure of VN_x films at all stages of their formation corresponds to the fcc structure of vanadium nitride.

3.2 The structure of already formed VN_x films of 1.5 μm -thickness

Fig. 4 shows SEM (a) and TEM (b) images of VN_x films deposited on silicon substrates. In the first case, the electron beam was directed at the film surface. In the second case, the sample was prepared by ion thinning of the end face of the substrate with the deposited film. It can be seen (Fig. 4, a) that film structure consists of blocks with a diameter of 150-250 nm. Blocks are non-homogeneous and consist of grains of irregular shape and size of 10-20 nm arbitrarily distributed in space.

The results of TEM study shown in Fig. 4, b confirm the SEM investigation data. The blocks are not homogeneous formations and consist of nano grains. The boundaries between blocks are loose; and the connections of 3-4 blocks contain pores of 5-10 nm in size.

In order to explore the structure and orientation of the individual grains in detail high resolution TEM (HRTEM) was used. Fig.5, a shows the area inside a single block. It can be seen that the block consists of nanograins of 5-15 nm size. Moreover, the crystallographic planes in each grain are arbitrarily oriented with respect to film plane.

It is difficult to calculate with high accuracy the interplanar spacings in each individual grain using Fig.5, a. To meet this challenge we used Fourier transformation of the diffraction peaks, which are responsible for the reflection from different crystallographic planes of the grains shown in Fig. 5.

Fig.5, b demonstrates the results of Fourier transformations and some interplanar spacing values. It can be seen that the grains are randomly distributed in the block volume. Parameter of fcc crystal lattice of VN_x film calculated on the base of interplanar spacing was 0.4052 nm.

3.3 Electrical and absorption characteristics

Taking into account the structural irregularity of VN_x films, the change of resistivity in the absorption and desorption processes can provide the important information about the pores state and kinetics of the hydrogen release from them. For multicomponent materials, the presence of gas-containing pores in such structure leads to the appearance of additional conduction mechanism which is either in the occurrence of thermionic conduction electrons due to emission from the gaseous impurities (nitrogen, oxygen) located on the pore surfaces and/or volume, or due to the tunneling effect. Consequently, the resistivity of material, which pores in whole or in part are filled with gas, will be less than that for the material with vacuum pores. For this occasion the electrical resistivity of material will be determined by the scattering of electrons by phonons, and boundaries of nano-grains and nano-pores.

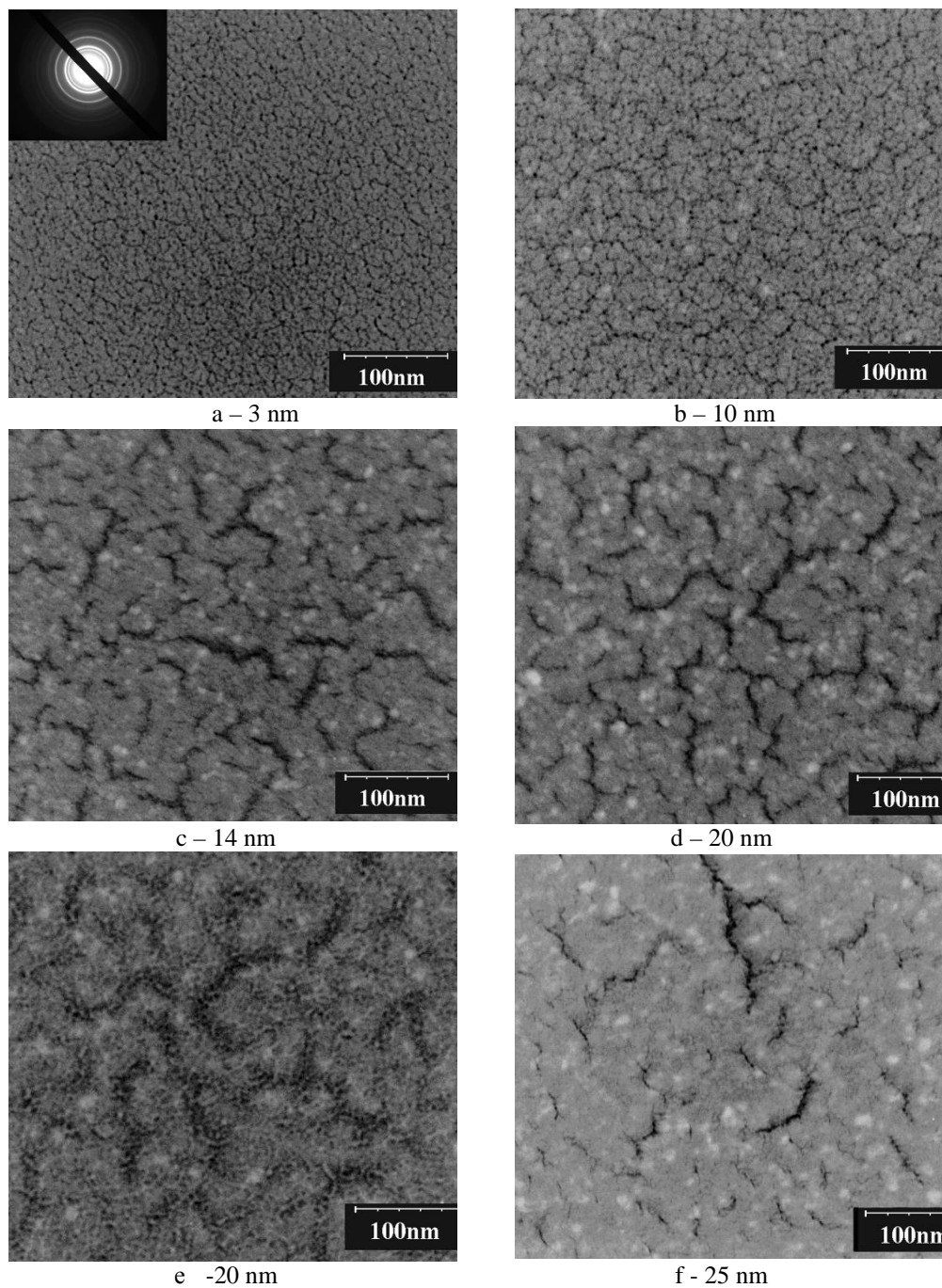


Figure 3. Electron-microscopy images of VN_x films structure at different deposition stages (the estimations for all film thicknesses are given).

Fig. 6 shows the corresponding dependences of VN_x film resistance on annealing temperature. It is seen that a decrease in resistance in the temperature range of 20-60°C is observed. It is typical for the films having a negative temperature coefficient of resistance. Further temperature increase causes an intense increase in resistance.

At 260°C the resistance of VN_x films is 10^4 times greater than the resistance of the hydrogen-saturated samples. In the cooling process resistance remains unchanged up to 180°C, and then decreases. The final value of resistance is 15-20% less than the resistance of the films saturated with hydrogen.

Fig.7 shows the hydrogen desorption curves indicating that the change in resistance of the films during annealing is uniquely related to the amount of hydrogen absorbed by them.

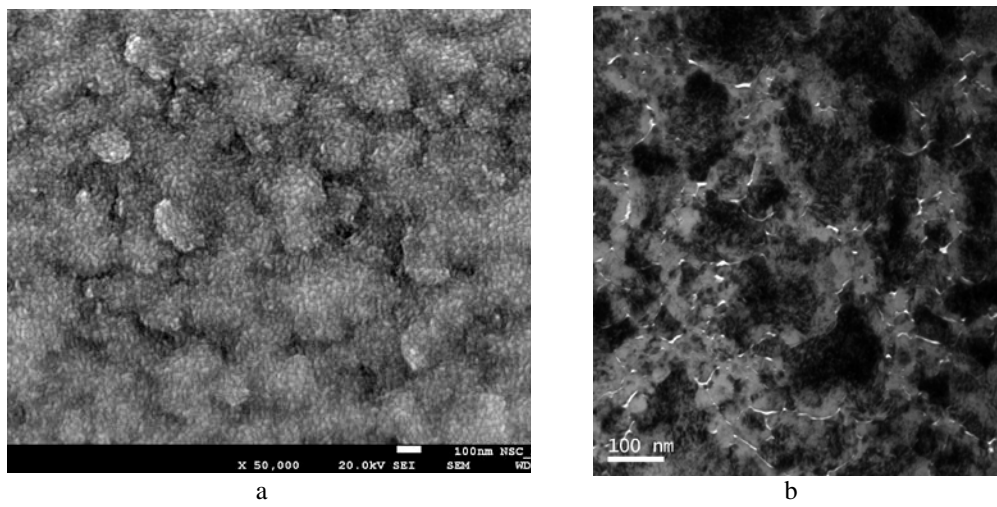


Figure 4. The structure of the surface (a), blocks and interblock boundaries (b) of already formed VN_x film.

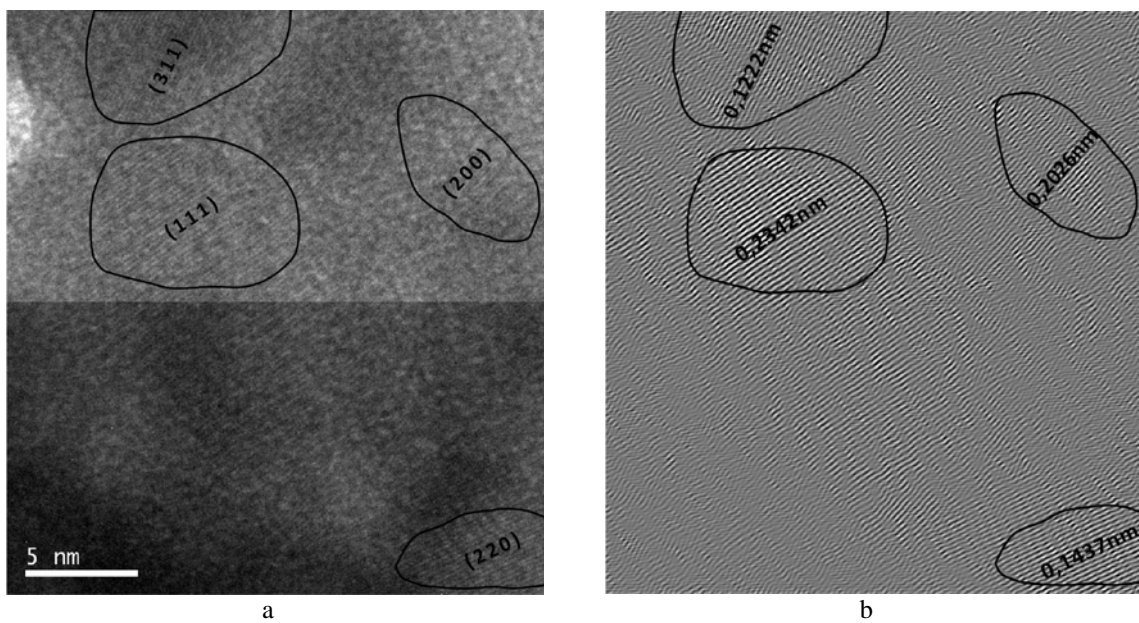


Figure 5. TEM image inside the block structure of VN_x film (a) and its Fourier transformation (b).

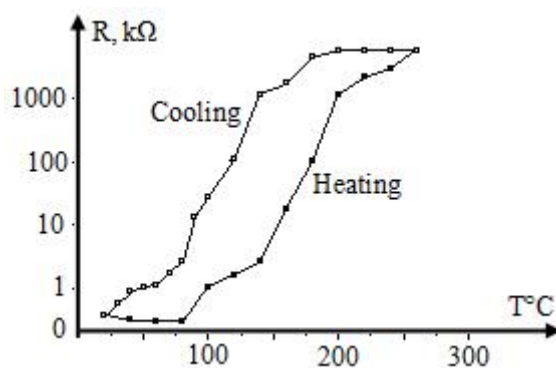


Figure 6. Changes in electrical resistance of VN_x films saturated with hydrogen during heating and cooling.

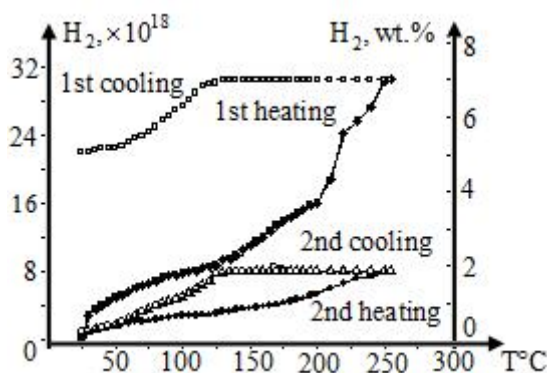


Figure 7. Dependences of the hydrogen amount in the annealing chamber during the initial annealing and reheating of $\text{VN}_x\text{-H}_y$ film. Reheating was performed after evacuation of hydrogen from the chamber

It was observed that the inflections of the primary annealing curve are correlated with the inflections in the dependence of the film resistance on the heating temperature (Fig. 6). Therefore, as the hydrogen release occurred, an increasing number of pores appears in the film; and the scattering of electrons on them leads to the gradual increase in film resistance. Reduction of VN_x film resistance during cooling corresponds to the received data on hydrogen absorption from the atmosphere inside the chamber and filling the open pores by hydrogen.

4 Discussion

Vanadium deposition under the ion-stimulated bombardment with working ion source occurs at a total pressure of nitrogen and helium in the chamber equaled to $(1.5\text{-}2.0)\times 10^{-3}$ Pa. At this pressure, the continuous adsorption of nitrogen molecules and helium atoms by the substrate surface is taking place simultaneously with the vanadium vapor deposition. Moreover, at such experimental conditions the rate of gases adsorption is not less than the speed of vanadium deposition. The partial dissociation of nitrogen molecules is in process at ion bombardment. Taking into account that Gibbs free energy of vanadium nitride formation is rather low [15], an ongoing chemisorption of nitrogen atoms and formation of vanadium nitride occurs. This may explain the vanadium nitride appearance at very early stages of film growth.

Physical adsorption of nitrogen molecules leads to the inhibition of diffusion processes on the film surface. As a result, there is a large-scale nucleation of small grains poorly oriented relatively to each other whose boundaries are saturated with nitrogen molecules and helium atoms. Radiation-induced diffusion of adsorbed gas atoms implanted at the irradiation stimulates the steady flow of gas molecules

and atoms to the grain boundaries. At a certain stage of the film growth, the amount of gas impurities in grain boundaries and in triple grain boundary intersections becomes sufficient for destruction of boundaries and for the formation of ruptures of 50-100 nm in length (Fig. 3b, c, d). This size is very close to the size of blocks shown in Fig. 4. Therefore, we believe that the formation of randomly distributed blocks is associated with the formation of such ruptures. The nucleation of new grains in the fracture areas prevents the formation of continuous columnar structure that is characteristic for the film deposition at a low-energy ion bombardment [4,5]. Fig. 8 shows the corresponding image of VN_x film cross-cut.

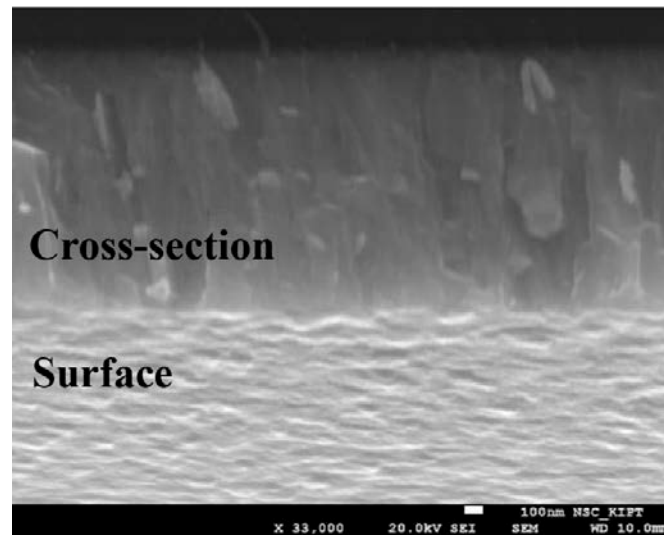


Figure 8. SEM image of the cross-section and the surface of VN_x film.

Quantitative analysis of the SEM results revealed that the nitrogen concentration in VN_x films does not exceed 10 at.%, although the selected-area electron-diffraction analysis shows the presence of nitride phase at all stages of film growth.

As noted above, the vanadium nitride formation at the initial stages of film growth may occur due to the adsorption of nitrogen molecules from the volume inside the vacuum chamber, their dissociation and nitride phase formation. The structure of VN_x film formed during the ion bombardment is nanocrystalline. Therefore, it is not necessary to provide equal amounts of vanadium and nitrogen for the nitride phase formation in such small grains.

It is known that during the transition from a polycrystalline to a nanocrystalline structure the fraction of the grain surface area in which the equilibrium vacancy concentration is different from concentration in "bulk" sample increases. The equilibrium concentration of vacancies in the small size particle depends on the particle size (r) as follows [16]:

$$C_s = C_v \exp(3\sigma\Omega/rkT) ,$$

where σ is the surface energy, and Ω is the atomic volume.

It follows from this expression that the equilibrium concentration of vacancies in small size particles may exceed significantly the concentration of vacancies in the "bulk" samples. A similar relationship exists for the diffusion coefficients too.

Increase in the equilibrium concentration of vacancies in nanograins of two-component structure like vanadium nitride can occur exclusively at the expense of nitrogen atom. Consequently, VN stoichiometric compound exists only in the central region of grains, and nitrogen is virtually non-existent in the grain boundaries. In this spirit, we believe that vanadium nitride with fcc-lattice exists in our films in the form of non-stoichiometric compound VN_x ($x < 1$).

Helium ions during film deposition penetrate deeper than a typical block size, namely, up to 250 nm (Fig.1, b). Rutherford backscattering and the thermal desorption spectra analysis we used to determine the He concentration but Helium was not observed in the analyses. The lack of helium indicates a good

gas permeability of formed porous nanocrystalline structure. The successive accumulation of helium atoms implanted by ion beam in film region which is at a distance of 80 to 250 nm from its surface takes place during VN_x film growth. As a result, local heating of the film in the damage zone and helium pressure increase inside it takes place. Helium implanted inside nanograins can easily move to the grain and interblock boundary surfaces and finally leave the film volume to high equilibrium concentration of vacancies in the nanograins and radiation-induced diffusion. Thus, the role of helium in the formation of solid-state VN_x hydrogen storage is to form nanopores linked by inter-granular and interblock boundaries. The role of nitrogen is to create vanadium bcc-structure that is denser than nanocrystalline fcc-structure of VN_x .

At the physical adsorption of hydrogen by such structures, rapid filling of grain boundaries and pores takes place. Further, a part of hydrogen molecules is dissociated in the grain boundaries and the diffusion of hydrogen atoms into them occur with the increase of pressure in the pores. The selected-area electron-diffraction data have not revealed the appearance of hydride phase. Therefore, the most likely and effective traps for hydrogen atoms are the vacant positions in VN_x lattice. It was shown for TiC_x [17, 18] that the greater the degree of deviation from stoichiometry ($x < 0.6$) is observed the greater amount of hydrogen atoms can be accumulated within the crystal lattice.

The configuration of nano pores in the investigated film structures is not just a system of voids that directly traverse each other. In the present case the pores are interconnected by relatively long intergranular boundaries of width that does not exceed 1 nm. This value is very closely related to the most optimal (0.6 nm) design size at which hydrogen will be retained in its molecular state [19]. The availability of such branched pore system connected by narrow and long channels provides the rapid delivery of molecular hydrogen to the film volume and its retention at room temperature.

5 Conclusion

The results given in this paper show that the use of IBAD method allows not only the controlled formation of nanoporosity with prescribed parameters but also the embedment of this nanoporosity into the nanocrystalline structure of a matrix. The material produced under such a method is capable to accumulate hydrogen at low pressures and room temperature. These structures can absorb the hydrogen up to 7 wt. % and release it in the temperature range of 50-275°C. The availability of broad channels between grains provides high diffusion mobility, which allows accumulating the hydrogen and releasing it from material within a short period of time. The formed structure accumulates hydrogen both in nanopores and in the vacancy (nitrogen empty) sites inside VN_x grains. Varying the basic parameters of the ion beam-assisted process and firstly its radiation component it is possible to produce nanocrystalline porous structures which will be suitable to uptake hydrogen in a high quantities and desorb it at the temperature no more than 100°C.

References

1. B. A. Movchan and A. V. Demchishin, "Investigation of the structure and properties of the thick vacuum kondesatov nickel, titanium, tungsten, aluminum oxide and zirconium dioxide," *The Physics of Metals and Metallography* (Russian) vol. 28, no. 4, pp. 653-660, 1969.
2. J. A. Thornton, "Influence of apparatus geometry and deposition conditions on the structure and topography of thick sputtered coatings," *Journal of Vacuum Science and Technologies*, vol. 11, pp. 666-670, 1974.
3. P. Barna and M. Adamik, "Fundamental structure forming phenomena of polycrystalline films and the structure zone models," *Thin solid films*, vol. 317, pp. 27-33, 1988.
4. J. E. Greene, S. A. Barnett, J.-E. Sundgren, and A. B. Rocket, *Ion Beam Assisted Film Growth*. Chap. 5, Elsevier, Amsterdam, 1989.
5. I. Petrov, P. Barna, I. Hultman, and J. Greene, "Microstructural evolution during film growth," *Journal of Vacuum Science and Technology*, vol. A21, no. 5, pp. S117- S128, 2003.
6. S. Dhara. Formation, Dynamics, and Characterization of nanostructures by ion beam irradiation. *Critical reviews in solid state and material sciences*, v.32, no. 1-2, pp.1-50, 2007.
7. A. Guglya, I. Marchenko, "Ion beam-assisted deposition," in *Comprehensive guide for nanocoatings technology*. NOVA press, USA, 2015.

8. W. Ensinger, "Low energy ion assists during deposition – an effective tool for controlling thin film microstructure," *Nuclear Instruments and Methods in Physics Researches*, vol. B127-128, pp. 796-808, 1997.
9. G. Wolf, "Modification of chemical properties of materials by ion beam mixing and ion beam assisted deposition," *Journal of Vacuum Science & Technologies*, vol. A10, no. 4, pp. 1757-1764, 1992.
10. A. Guglya, I. Marchenko, and I. Neklyudov, "Chromium film deposition stimulated by nitrogen ions implantation with energies up to 30 keV," *Surface Coating Technologies*, vol. 173-174, pp. 1248-1252, 2003.
11. K. Volz, M. Kiuchi, and W. Ensinger, "Structural investigations of chromium nitride films formed by ion beam-assisted deposition," *Surface Coating Technologies*, vol. 108-109, pp. 303-307, 1998.
12. I. Jain, Y. Vijay, L. Malhotra, and K. Uppadhyay, "Hydrogen storage in thin film metal hydride - a review," *International journal of Hydrogen Energy*, vol. 13, pp. 15-23, 1988.
13. K. Papathanassopoulos and H. Wenzl, "Pressure-composition isotherms of hydrogen and deuterium in vanadium films measured with a vibrating quartz microbalance," *Journal Physics F: Metal Physics*, vol. 12, pp.1369-138, 1982.
14. V. Bendikov, A. Guglya, I. Marchenko, D. Malykhin, and I. Neklyudov, "Mechanisms of forming the Cr-N composite in the unsteady-state stage of ion beam-assisted deposition process," *Vacuum*, vol. 70, pp. 331-337, 2003.
15. I.Takano, S.Isobe, T.Sasaki, Y.Baba, Nitrogenation of various transition metals by N_2^+ - ion implantation, *Appl. Surf. Science*. vol. 37, pp. 25-32, 1989.
16. T. Gladkih, S. V. Gukarov, A. P. Kryshthal, V. I. Larin, V. N. Suhov, and S. I. Bogatyrenko, *Surface phenomena and phase transitions in condensed films* (Russian), Kharkov, KhNU, 2004
17. A. Gringoz, N. Glandu, and S. Valette, "Electrochemical hydrogen storage in $TiC_{0.6}$, not in $TiC_{0.9}$," *Electrochemistry Communications*, vol. 11, pp. 2044-2047, 2009.
18. H. Ding, X. Fan, C. Li, X. Liu, D. Jiang, and C. Wang, "First-principles study of hydrogen storage in non-stoichiometric TiC_x ", *Journal Alloys and Compounds*, vol. 551, pp. 67-71, 2013.
19. I. Carbia, M. Lopez, and J. Alonso, "The optimum average nanopores size hydrogen storage in carbon nanoporous materials," *Carbon*, vol. 45, pp. 2649-2658, 2007.